

OPEN ACCESS

EDITED BY

Yansheng Zhang,
Shanghai University,
China

REVIEWED BY

Archana Giri,
Jawaharlal Nehru Technological University,
India
Dongming Ma,
Guangzhou University of Chinese Medicine,
China

*CORRESPONDENCE

Jinhui Wang
wangjinhui@hrbmu.edu.cn
Jian Huang
huangjian@hrbmu.edu.cn

SPECIALTY SECTION

This article was submitted to
Plant Metabolism and Chemodiversity,
a section of the journal
Frontiers in Plant Science

RECEIVED 29 May 2022

ACCEPTED 15 August 2022

PUBLISHED 10 October 2022

CITATION

Qu LY, Gan CL, Cheng XL, Lin CC, Wang YL,
Wang LB, Huang J and Wang JH (2022)
Discovery of physalin biosynthesis and
structure modification of physalins in
Physalis alkekengi L. var. *franchetii*.
Front. Plant Sci. 13:956083.
doi: 10.3389/fpls.2022.956083

COPYRIGHT

© 2022 Qu, Gan, Cheng, Lin, Wang, Wang,
Huang and Wang. This is an open-access
article distributed under the terms of the
Creative Commons Attribution License
(CC BY). The use, distribution or
reproduction in other forums is permitted,
provided the original author(s) and the
copyright owner(s) are credited and that
the original publication in this journal is
cited, in accordance with accepted
academic practice. No use, distribution or
reproduction is permitted which does not
comply with these terms.

Discovery of physalin biosynthesis and structure modification of physalins in *Physalis alkekengi* L. var. *franchetii*

Liyuan Qu, Chunli Gan, Xiaoling Cheng, Congcong Lin,
Yanli Wang, Libo Wang, Jian Huang* and Jinhui Wang*

Department of Pharmaceutical Chemistry, College of Pharmacy, Harbin Medical University, Harbin, China

Physalins, active ingredients from the *Physalis alkekengi* L. var. *franchetii* (*P. alkekengi*) plant, have shown anti-inflammatory, antioxidant and anticancer activities. Whereas the bioactivity of physalins have been confirmed, their biosynthetic pathways, and those of quite a few derivatives, remain unknown. In this paper, biosynthesis and structure modification-related genes of physalins were mined through transcriptomic and metabolomic profiling. Firstly, we rapidly and conveniently analyzed physalins by UPLC-Q-TOF-MS/MS utilizing mass accuracy, diagnostic fragment ions, and common neutral losses. In all, 58 different physalin metabolites were isolated from *P. alkekengi* calyxes and berries. In an analysis of the physalin biosynthesis pathway, we determined that withanolides and withaphysalins may represent a crucial intermediate between lanosterol and physalins. and those steps were decanted according to previous reports. Our results provide valuable information on the physalin metabolites and the candidate enzymes involved in the physalins biosynthesis pathways of *P. alkekengi*. In addition, we further analyzed differential metabolites collected from calyxes in the Jilin (Daodi of *P. alkekengi*) and others. Among them, 20 physalin metabolites may represent herb quality biomarkers for Daodi *P. alkekengi*, providing an essential role in directing the quality control index of *P. alkekengi*.

KEYWORDS

Physalins, plant metabolomics, biosynthetic pathways, Daodi medicinal materials, *Physalis alkekengi* L var. *franchetii* (mast.) Makino

Introduction

Medicinal plants provide humans with a valuable source of potential therapeutic agents. Historically, physalis plants such as *Physalis alkekengi* L. var. *franchetii* (*P. alkekengi*) have been used to treat inflammation for centuries (Li et al., 2018). Their anti-inflammatory properties are based on the production of physalins (Shu et al., 2016). The physalin skeleton

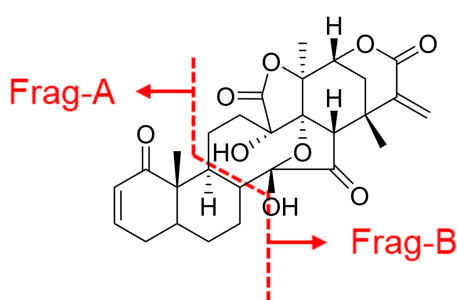


FIGURE 1
The skeleton of physalins. The skeleton of physalins was split into two parts, Frag-A and Frag-B. Frag-A is comprised of 2 six-membered ring molecules, where 1-C is the carbonyl group. Frag-B is comprised of four parts, where 27-C and 14-OH are likely to form rings or annular structures.

has been found to be an extraordinarily complex, 13–14 secosteroid skeleton incorporating a nine-membered carbocycle derived from a steroidal ring fused to a six-membered ring with δ -lactone (Sun et al., 2017). These complexes are the structural basis of physalin, which has been studied for more than half a century. Differences between physalins, replace substituents with those bearing different electromagnetic charges. Other major differences are located in 27-C, such as in physalin A and physalin G. Based on this, the skeleton of physalins was split into two parts, Frag-A and Frag-B (Figure 1). Frag-A is comprised of 2 six-membered ring molecules, where 1-C is the carbonyl group. Frag-B is comprised of four parts, where 27-C and 14-OH are likely to form rings or annular structures. Physalins are mainly found in plants of the genus *Physalis* (Li et al., 2014; Wu et al., 2020; Xu et al., 2013), and they are biologically active, that is, they can inhibit tumor growth (Zhu et al., 2016), suppress lymphocyte proliferation (Ding et al., 2020), and inhibit inflammatory processes (Wu et al., 2012). Physalins are a potential source of targeted drug libraries due to their variety and complexity in structures and types of compounds.

Plants possess a diverse array of metabolic products arising from both primary and secondary metabolisms. Plant metabolomics involves the comprehensive analysis of plant metabolites and secondary metabolism (Last et al., 2007; Sawada et al., 2009; Urano et al., 2010). The plant metabolome is regarded as the bridge connecting the genome with the phenome (Luo, 2015). Based on this, the correlation between chemical composition and biosynthesis could be established by plant metabolomics. It offers a source of information about the physiological status of plants (Oikawa et al., 2015). The main strategies in plant metabolomics studies are metabolic fingerprinting and metabolite profiling (Dunn and Ellis, 2005). Spectral characteristics, sensitivity, and quantification of metabolomics are primarily addressed by mass spectrometry (MS) and nuclear magnetic resonance (NMR) spectroscopy. Recent years have seen a rapid advancement in liquid chromatography and mass spectrometry systems that have driven plant metabolomics (Sawada and Yokota Hirai, 2013).

Previous studies of physalin biosynthetic pathways have concentrated on biosynthetic-related genes. The first reported study on biosynthesis of physalins was carried out by Fukushima et al. (2016), where 24-methylidesmosterol was designated as a key intermediate in physalin biosynthesis (Fukushima et al., 2016). Relevant studies were continually advanced, withanolide were designated as the new key intermediate physalin biosynthesis (Knoch et al., 2018; Yang et al., 2022b). However, the key steps for progress from 24-methylidesmosterol to physalins is still unexplored (Figure 2).

The purpose of this study is to follow-up research based on the previous studies. Further data mining of their RNA Sequencing data was performed to interpret the physalin biosynthesis pathway in *P. alkekengi* (Fukushima et al., 2016). Our view of physalin biosynthesis was based upon the structural characterization of physalin in *P. alkekengi*. Plant metabolomics helps to dissect primary and secondary metabolites. Based on the cleavage rules of physalins, our research team used UPLC-Q-TOF-MS/MS to detect structural diversity in physalins. In the present study, 58 physalin metabolites were identified. Through data mining using the online database, a further analysis of the biosynthesis pathway for physalins is presented here. Collectively, the modification of physalin skeletons is achieved by desaturation, methylation, hydroxylation, epoxidation, cyclization, chain elongation, and glycosylation, etc. Finally, we compare the differences of major physalins between geographically diverse calyxes of *P. alkekengi*.

Materials and methods

Chemicals and reagents

Acetonitrile (MS grade) and formic acid (LC-MS grade) were all purchased from Thermo Fisher Scientific Corporation. Other chemicals and reagents were analytical grade and commercially available. The standard substances physalin A, physalin D, physalin G, physalin L and physalin O (purity greater than 97%) were isolated and purified by our laboratory, and the method used for preparation of these standard substances has been described previously (Lin and Wang, 2011). All standards were dissolved in methanol and then diluted to a final concentration of 10 μ g/ml. Before use, all standard solutions were stored in glass storage vial at -20°C .

Plant material and sample preparation

Physalis alkekengi fruit collection took place across China in May and June of 2020. The fruits were rapidly isolated, immediately after being collected, and all samples were put on ice until they were transported to -80°C for storage. In total, 18 different regional fruits were collected. Sample information is shown in Table 1.

The calyxes and berries were separated manually, and extracted by ultrasonication. Each sample (~ 1 g) was extracted

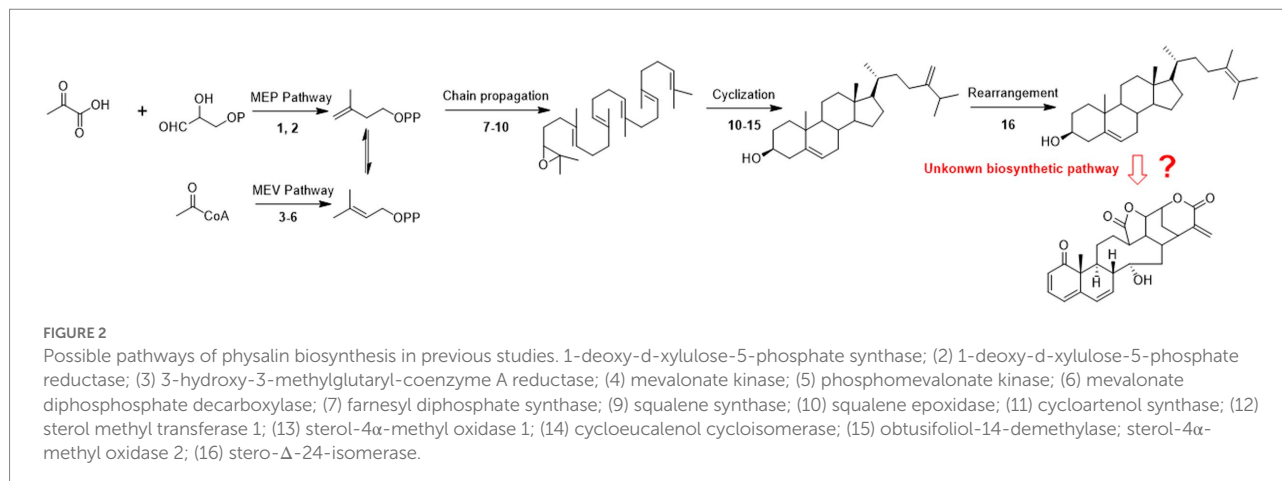


TABLE 1 Geographical distribution of sample information.

Samples No	Sample	Sample type	Origin (province)	Sampling time
20,210,506-PAC-HJL-01	<i>Physalis alkekengi</i> L.var.	Whole fruit	Heilongjiang	October
20,210,506-PAC-JL-01	<i>Physalis alkekengi</i> L.var.	Whole fruit	Jilin	October
20,210,506-PAC-NL-01	<i>Physalis alkekengi</i> L.var.	Whole fruit	Liaoning	October
20,210,506-PAC-SD-01	<i>Physalis alkekengi</i> L.var.	Whole fruit	Shandong	August
20,210,506-PAC-ZJ-01	<i>Physalis alkekengi</i> L.var.	Whole fruit	Zhejiang	August
20,210,506-PAC-JL-02	<i>Physalis alkekengi</i> L.var.	Whole fruit	Jilin	August
20,210,506-PAC-JL-03	<i>Physalis alkekengi</i> L.var.	Whole fruit	Jilin	August
20,210,506-PAC-HN-01	<i>Physalis alkekengi</i> L.var.	Whole fruit	Hunan	August
20,210,506-PAC-JL-04	<i>Physalis alkekengi</i> L.var.	Whole fruit	Jilin	August
20,210,506-PAC-JL-05	<i>Physalis alkekengi</i> L.var.	Whole fruit	Jilin	August
20,210,506-PAC-JL-06	<i>Physalis alkekengi</i> L.var.	Whole fruit	Jilin	August
20,210,506-PAC-JL-07	<i>Physalis alkekengi</i> L.var.	Whole fruit	Jilin	August
20,210,506-PAC-JL-08	<i>Physalis alkekengi</i> L.var.	Whole fruit	Jilin	August
20,210,506-PAC-JL-09	<i>Physalis alkekengi</i> L.var.	Whole fruit	Jilin	August
20,210,506-PAC-JL-10	<i>Physalis alkekengi</i> L.var.	Whole fruit	Jilin	August
20,210,506-PAC-JL-11	<i>Physalis alkekengi</i> L.var.	Whole fruit	Jilin	August
20,210,506-PAC-HN-02	<i>Physalis alkekengi</i> L.var.	Whole fruit	Hunan	August
20,210,506-PAC-HLJ-02	<i>Physalis alkekengi</i> L.var.	Whole fruit	Heilongjiang	August

with 10 ml of methanol at room temperature (25°C) for 30 min, the liquid supernatants were further processed by solid-phase extraction (SPE) by the following steps: The SPE was activated with methanol and then with water. After loading 1 ml of sample, the SPE was washed with 1 ml of methanol, and the filtrate was combined and retained for subsequent compositional analysis.

LC-MS/MS conditions

The metabolic profile of *P. alkekengi* calyxes and berries were determined by UPLC-Q-TOF MS/MS (Waters Corporation, Milford, MA, United States). Chromatography was performed on a UPLC system (Waters Corp., United States) with an autosampler at 4°C. The separations were carried out on an ACQUITY UPLC®

BEH C18 column (1.7 μ m, 2.1 \times 50 mm, Waters Corporation, United States). The column temperature was maintained at 45°C. The analysis was performed with gradient elution using (A) methanol and (B) water with 0.1% formic acid as the mobile phase: 0–4.5 min, 10–50% A; 4.5–11.5 min, 50–98% A; a work-loop with no injection was carried out before assaying samples for equilibration of the column. The flow rate was set to 0.4 ml/min. Throughout the analysis, all samples were kept at 4°C. A Waters Acquity™ Mass Spectrometer (Waters Corp., Milford, CT, United States) was connected to the UPLC system *via* an electrospray ionization (ESI) interface. The capillary voltage and sample cone voltage, source offset voltage and source temperature of positive modes were 3.0 kV, 40 V, 80 V, and 100°C, respectively. The desolvation temperature was 250°C. The cone and desolvation gas flow rates were 50 l/h and 600 l/h, respectively. The data

acquisition rate was set at 0.2 s/scan, with a 0.1 s (0.02 interscan time) interscan delay. MS data were collected in centroid mode from 50 to 1,000 Da. MS data were obtained by using MSE acquisition mode. For accurate mass acquisition, a lock-mass of leucine enkephalin was used to ensure accuracy through the whole MS analysis. Data were obtained by Masslynx 4.1 (Waters Corp., United States).

Data mining analysis

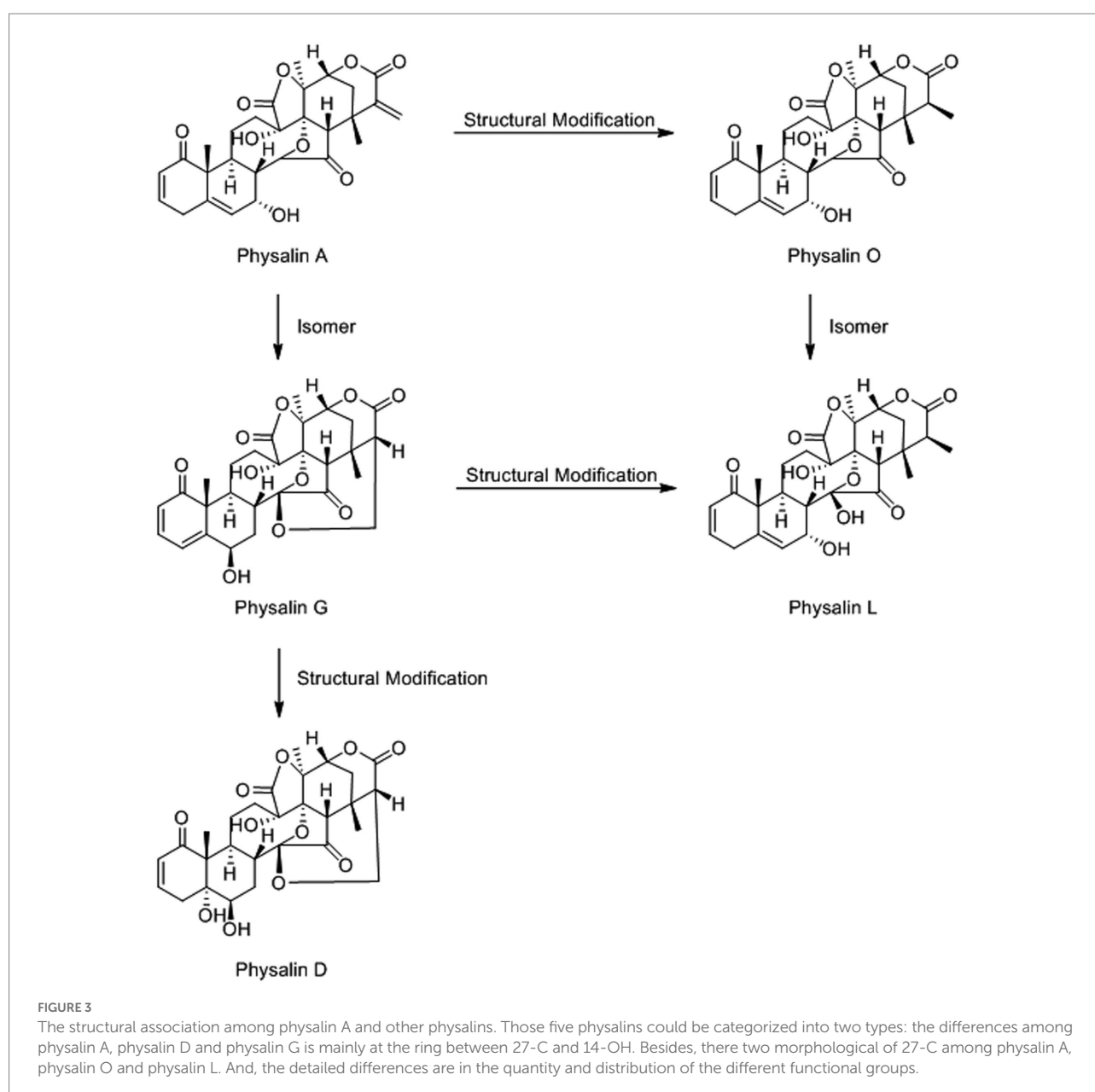
The data mining analysis was carried out using the commercial software Progenesis QI (Version 2.3, herein after referred to as QI) and UNIFI v1.9.3 software (Waters Corp.).

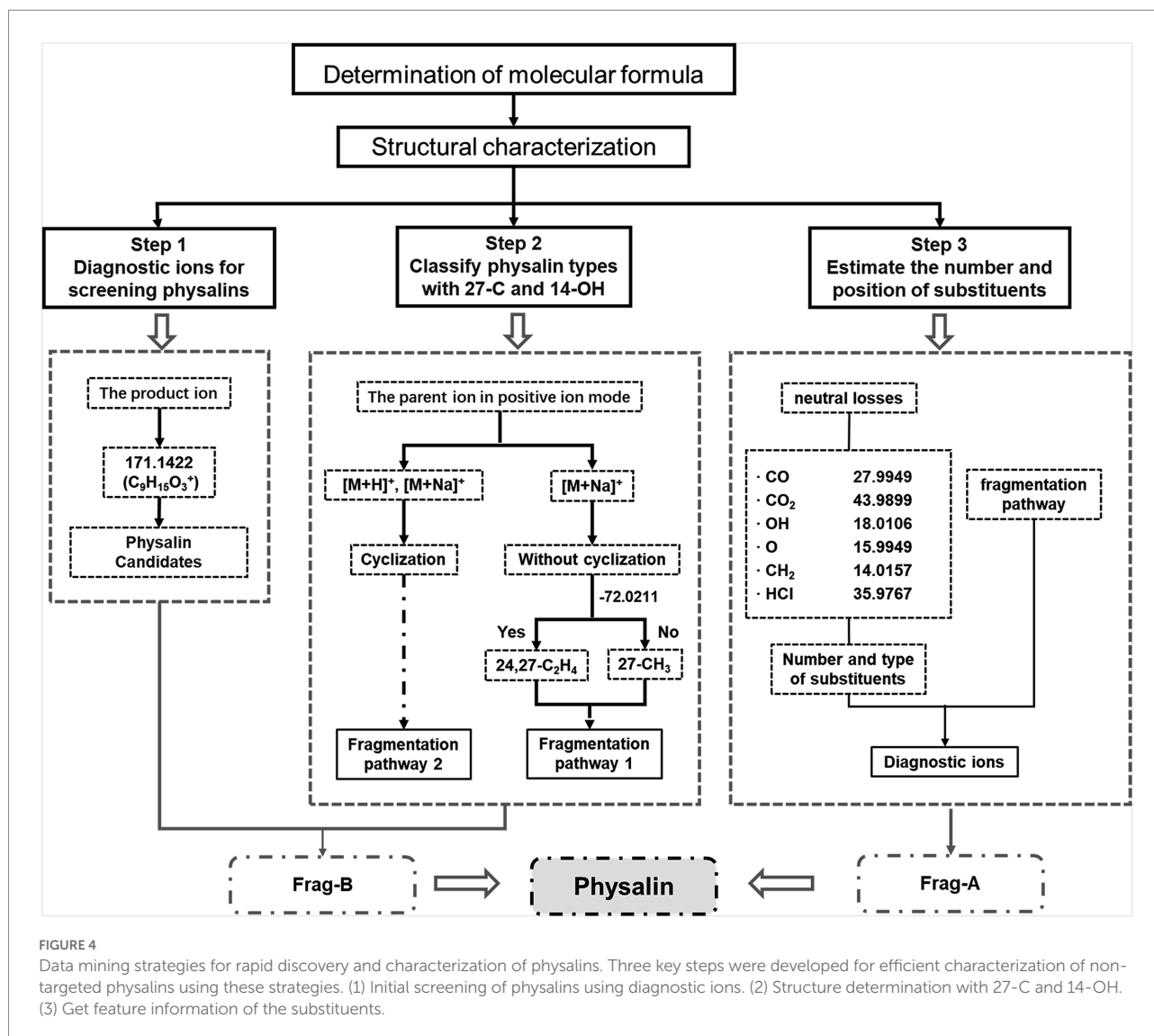
Identification of metabolites

Structural identification of the secondary phytochemicals (physalins) was based on different cleavage rules of physalins. We used several strategies, such as diagnostic fragmentation screening and fragment monitoring, during the process.

Statistical analysis

The raw data were imported into QI to be processed. This included peak annotation and normalization. Analysis of all metabolites between groups was performed. Multivariate statistical analysis was performed using orthogonal partial least squares-discriminant analysis (OPLS-DA) and variable importance in projection (VIP) of each metabolite was determined (EZinfo 3.0, an internal software program of Progenesis QI).





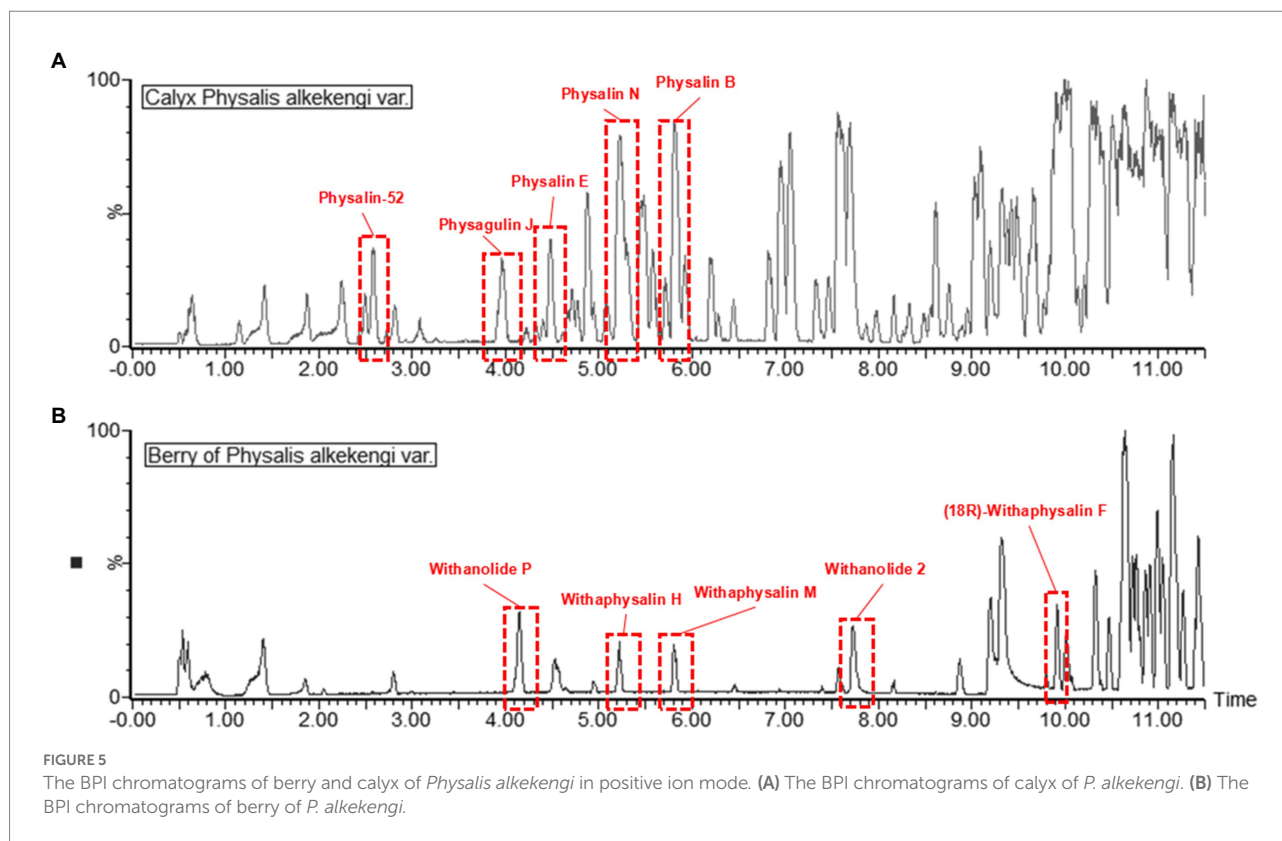
Results and discussion

Data mining strategies for rapid discovery and characterization of physalins

The structure of physalin is complex and covers a wide variety of structural deformation (Sun et al., 2017). This makes mass spectrometric identification difficult. To solve this problem, we employed a high-throughput method for physalin identification. Five physalin standards (physalin A, D, G, L and O) were investigated to ascertain their MS/MS fragmentation behaviors, providing a basis for structural elucidation of physalins. The structural association among physalin A and others is shown in Figure 3.

Based on the MS behaviors of the physalin standards (described in detail in the Supplementary Material), a high-efficiency approach using LC-MS/MS together with a data mining

strategy for rapid discovery and identification of non-targeted physalins in complex samples was proposed (Figure 4). Three key steps were developed for efficient characterization of non-targeted physalins using these strategies. The first key step was to screen physalins using diagnostic ions from Frag-B. 171.1422 was used as a diagnostic ion to screen precursor ions of physalin candidates. The second key step was to classify physalin types with 27-C and 14-OH. The cyclization between 27-C and 14-OH was judged by using parent ion data in positive ion mode. Then, the signature neutral loss of C₂H₄ and CO₂ (-72.0211) from Frag-B was used for identify the types of 27-C. The third key step was to estimate the number and position of substituents using neutral losses and diagnostic ions from Frag-A. Generally speaking, the number and varieties of substituents were determined by the neutral fragment losses. Then, the positions of substituents were determined by comprehensive information in diagnostic ions which included substituents and signature fragments.



The differential physalin metabolites in calyxes and berries of *Physalis Alkekengi*

Primary metabolites were present in nearly every tissue and involved in synthesis of secondary metabolisms (Oikawa et al., 2015). Conversely, specialized secondary metabolism is generally limited to specific stages of organism development and occurs in specialized tissues for specific functions (Yazaki, 2005). It has been found that fruits are the main sources of physalins in *P. alkekengi* (Yang et al., 2022a). For this reason, fresh berries were isolated from whole fruit and were detected under the same conditions as calyxes (Figure 5). In all, 58 different physalin correlative metabolites were detected based on the identification strategy above in *P. alkekengi* (Table 2). In our data analysis, physalin correlative metabolites are divided into three main categories, which are withanolides, withaphysalins and physalins.

In order to exclude interference from moisture while calculating the content for each ingredient, the quantitative analysis of all components was performed by area normalization using physalin D as the internal standard. Heatmaps of metabolites were drawn with the OmicStudio tools at <https://www.omicstudio.cn>. using unit UV and HCA (Figure 6). Using the identification criterion of the absolute $\text{Log}_2 \text{FC} \geq 1$, 46 physalin metabolite contents, including 32 upregulated metabolites and 14 downregulated metabolites, were found to be significantly different among the 58 physalin metabolites in berries vs. calyxes of *P. alkekengi*. We found that physalins are more

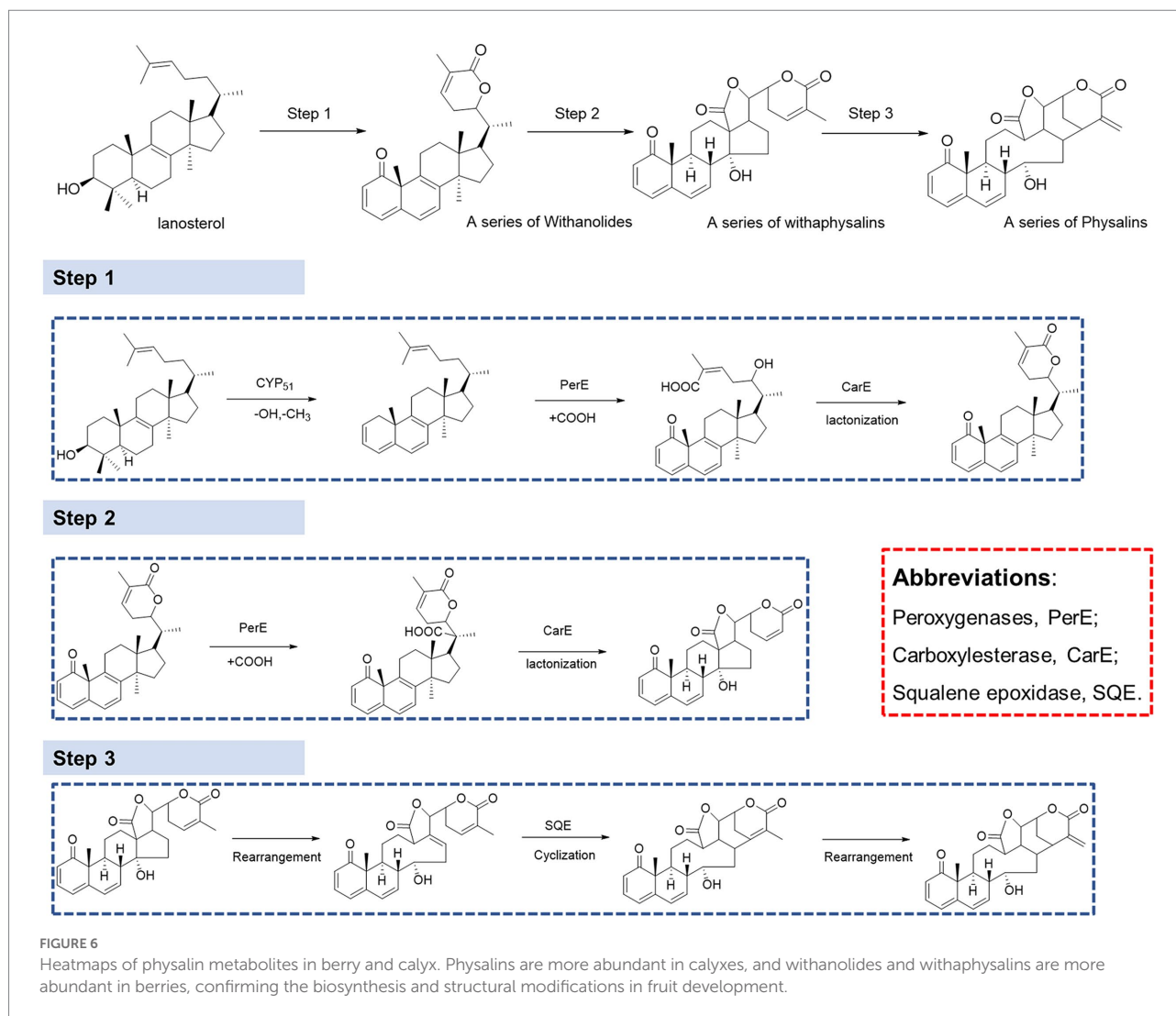
abundant in calyxes, and withanolides and withaphysalins are more abundant in berries, confirming the biosynthesis and structural modifications in fruit development. The berries are responsible for physalin synthesis, whereas the calyx is responsible for physalin accumulation in *P. alkekengi* berries (Table 3).

Biosynthetic pathway analysis of physalin metabolites in *Physalis Alkekengi*

It has been proven that physalin is well associated with mevalonate (MEV) and methylerythritol 4-phosphate (MEP) pathways, and that lanosterol is a key intermediate of the biosynthesis of physalins. However, there is still much that is unknown about the biosynthesis pathway from lanosterol to physalins (Fukushima et al., 2016). Withanolides and withaphysalins may represent an intermediate between lanosterol and physalins. To understand the molecular basis of physalin biosynthesis in *P. alkekengi*, transcriptomes were analyzed. We downloaded the Supplementary Material of transcriptomes from earlier literature (Fukushima et al., 2016), and molecular reclassification and identification of biosynthetic gene clusters for physalin metabolites. They discovered 40,090 UniGenes specific to *P. alkekengi*. Based on the results of physalin correlative metabolites, the synthesis of physalins can be divided into three steps (Figure 7).

TABLE 2 Summary of the physalins metabolites identification results.

RT (min)	m/z	Mass error (ppm)	Formula	Compounds name	Pubchem ID
0.56	997.5366	2.50	C ₂₉ H ₃₈ O ₇	Physaminimin A	102,223,242
2.57	591.3134	7.61	C ₃₂ H ₄₆ O ₁₀	Physalin-52	60,005,230
3.70	565.2755	-0.38	C ₃₁ H ₄₂ O ₈	Physalin-09	140,492,210
3.93	531.2913	5.98	C ₃₀ H ₄₂ O ₈	Physagulin J	42,610,742
4.10	477.2638	-1.38	C ₂₈ H ₃₈ O ₅	Withanolide P	21,679,034
4.16	495.2717	0.23	C ₂₈ H ₄₀ O ₆	Vamonolide	13,939,886
4.18	577.2063	-1.38	C ₃₀ H ₃₄ O ₁₀	Physalin V	102,254,402
4.24	565.1662	-1.96	C ₂₈ H ₃₀ O ₁₁	Physalin-109	162,827,760
4.24	545.2044	4.76	C ₂₈ H ₃₂ O ₁₁	Physalin D	431,071
4.75	527.1919	-3.91	C ₂₈ H ₃₀ O ₁₀	Isophysalin A	57,387,832
4.75	567.1834	1.31	C ₂₈ H ₃₂ O ₁₁	Physalin E	13,962,952
4.90	583.1758	-4.51	C ₂₈ H ₃₂ O ₁₂	physalin-02	140,498,412
4.95	549.1731	-0.05	C ₂₈ H ₃₀ O ₁₀	Physalin J	44,426,449
4.99	513.1763	5.95	C ₂₇ H ₂₈ O ₁₀	Physalin-83	42,617,138
5.10	569.1986	0.88	C ₂₈ H ₃₄ O ₁₁	Physalin 2	140,646,467
5.10	529.2090	0.32	C ₂₈ H ₃₂ O ₁₀	Physalin L	146,156,484
5.17	553.2037	-2.92	C ₂₈ H ₃₄ O ₁₀	Physalin-17	91,351,492
5.17	513.2073	-9.06	C ₂₈ H ₃₂ O ₉	25,26-Epidihydrophysalin C	42,610,672
5.22	965.5406	-3.25	C ₂₉ H ₃₈ O ₆	Withaphysalin H	21,606,682
5.23	549.1733	5.48	C ₂₈ H ₃₀ O ₁₀	Physalin N	131,752,539
5.32	503.3031	3.33	C ₂₉ H ₄₂ O ₇	2,3-Dihydro-3beta-methoxy withaferin A	10,767,792
5.35	583.1800	5.81	C ₂₈ H ₃₂ O ₁₂	Physalin-66	58,594,640
5.59	549.1733	3.15	C ₂₈ H ₃₀ O ₁₀	Physalin F	49,864,133
5.75	505.2184	6.65	C ₂₈ H ₃₄ O ₇	Withaphysalin M	10,096,775
5.83	549.1728	0.28	C ₂₈ H ₃₀ O ₁₀	Physalin X	102,319,017
5.86	533.1787	1.44	C ₂₈ H ₃₀ O ₉	Physalin B	11,613,161
5.92	581.1993	-0.06	C ₂₉ H ₃₄ O ₁₁	Physalin I	131,751,562
5.93	549.1731	1.94	C ₂₈ H ₃₀ O ₁₀	Physalin Z	44,577,484
6.01	563.1926	7.01	C ₂₉ H ₃₂ O ₁₀	Physalin-120	163,183,929
6.05	535.1940	-6.00	C ₂₈ H ₃₂ O ₉	Physalin M	76,900,148
6.32	523.2286	0.39	C ₂₈ H ₃₆ O ₈	Withaperuvine E	85,089,867
6.71	489.2247	-3.10	C ₂₈ H ₃₄ O ₆	Withaphysalin A	14,216,298
6.96	533.1779	0.45	C ₂₈ H ₃₀ O ₉	Isophysalin B	22,748,169
7.12	549.1732	-5.08	C ₂₈ H ₃₀ O ₁₀	Physalin U	44,577,487
7.14	507.2344	0.35	C ₂₈ H ₃₆ O ₇	Withaphysalin N	11,752,064
7.14	467.2407	-0.52	C ₂₈ H ₃₄ O ₆	Withaphysalin A	14,216,298
7.31	489.2254	4.26	C ₂₈ H ₃₄ O ₆	Withaphysalin P	102,471,581
7.34	507.2354	1.50	C ₂₈ H ₃₆ O ₇	(18S)-Withaphysalin F	21,606,679
7.45	489.2250	-0.26	C ₂₈ H ₃₄ O ₆	Withaphysalin J	21,606,684
7.61	587.2869	6.92	C ₃₂ H ₄₂ O ₁₀	Withanolide 2	101,005,225
7.61	547.2141	-9.34	C ₂₈ H ₃₄ O ₁₁	Physalin-35	90,264,481
7.99	577.2307	-2.22	C ₂₉ H ₃₆ O ₁₂	Physalin G	11,017,274
9.11	487.2679	4.09	C ₂₈ H ₃₈ O ₇	Withanolide E	301,751
9.86	969.5062	-2.89	C ₂₈ H ₃₆ O ₇	(18R)-Withaphysalin F	21,606,678
10.20	625.3374	4.45	C ₃₄ H ₅₀ O ₉	Physapruin B	131,752,899
10.25	707.3253	4.74	C ₃₆ H ₅₀ O ₁₄	Physagulin E	10,009,993
10.45	523.2926	-3.32	C ₂₈ H ₄₂ O ₆	Physangulide	14,605,176
10.60	945.5771	-0.10	C ₂₈ H ₄₀ O ₆	Ixocarpanolide	14,605,184
10.64	523.2696	-7.43	C ₂₉ H ₄₀ O ₇	Withaphysalin R	102,471,583
10.80	961.5007	0.13	C ₂₉ H ₃₆ O ₆	Withaphysalin K	21,606,685
10.81	977.5583	-0.06	C ₂₈ H ₄₀ O ₇	14alpha-Hydroxyixocarpanolide	14,605,187
11.00	543.1897	1.92	C ₂₈ H ₃₀ O ₁₁	25-Hydroxy physalin F	73,350,641
11.15	531.2993	-4.97	C ₃₀ H ₄₂ O ₈	Physaminimin F	102,223,246
11.16	543.1882	4.82	C ₂₈ H ₃₀ O ₁₁	25-Hydroxy physalin J	73,346,012
11.20	977.5640	5.11	C ₂₈ H ₄₀ O ₇	3-HDH-withanolide F	135,887
11.41	909.5485	-2.69	C ₂₈ H ₃₈ O ₅	Withanolide P	21,679,034
11.44	933.4787	-0.12	C ₂₈ H ₃₄ O ₆	Withaphysalin D	101,293,641
11.44	569.3625	3.93	C ₃₆ H ₅₀ O ₄	Physanol A	102,067,218



In step 1, lanosterol generates withanolides with hydroxylation, lactonization, demethylation, and dehydrogenation, this is the first step toward the synthesis of physalins in plants. As steroidal lactones, withanolides are natural compounds that are formed when the oxo- and carbo-xylic groups of C22 and C26 are combined to form a six-membered lactone ring (Misico et al., 2011). In previous studies, it had been observed that methyltransferase and cytochrome P450 are main enzymes involved in the withanolides biosynthesis pathway (Gupta et al., 2015). Demethylation of lanosterol can be performed by demethylase hydroxylation or the hydroxyl radical damage of the methyl group (Mishra et al., 2019). Of all the genes, there are a total of 16 demethylases. Sterol 14 α -demethylase (CYP51) belongs to the superfamily of cytochrome P450, which are the enzymes essential for sterol biosynthesis (Kim et al., 2005). CYP51 may potentially be the demethylase enzyme in this step. After demethylation, macrolactonization followed by ring-closing metathesis are the key steps. In this respect, peroxygenases and carboxylesterase represent a promising solution. This observation was further confirmed by observation that carboxylic acid derivatives of plant sterols were presented in our result. Peroxygenases are reported to catalyze

hydroxylation (Babot et al., 2015). And carboxylase became the main enzyme responsible for the carboxylation reaction (Pontrelli et al., 2018; Roesler et al., 2021). Next, withanolides generate withaphysalins with hydroxylation and lactonization, which can be performed by peroxygenase and carboxylesterase enzymes. This is the second step toward the synthesis of physalins in plants. Finally, Michael rearrangement and cyclization reactions prompt the final synthesis of physalins, and is the third and paramount step toward the synthesis of physalins in plants. After physalin skeletons are formed, biochemical reactions (e.g., desaturation, methylation, hydroxylation, epoxidation, cyclization, chain elongation, and glycosylation) lead to various biochemical products of physalin skeletons.

Physalin metabolites in geographically diverse calyces of *Physalis Alkekengi*

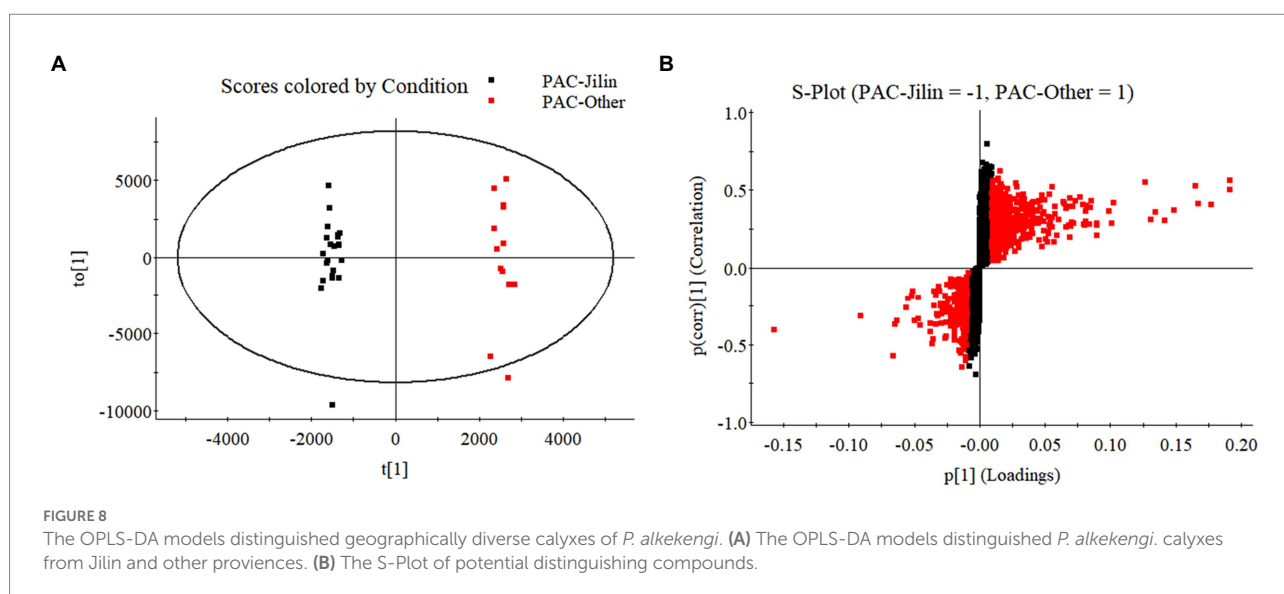
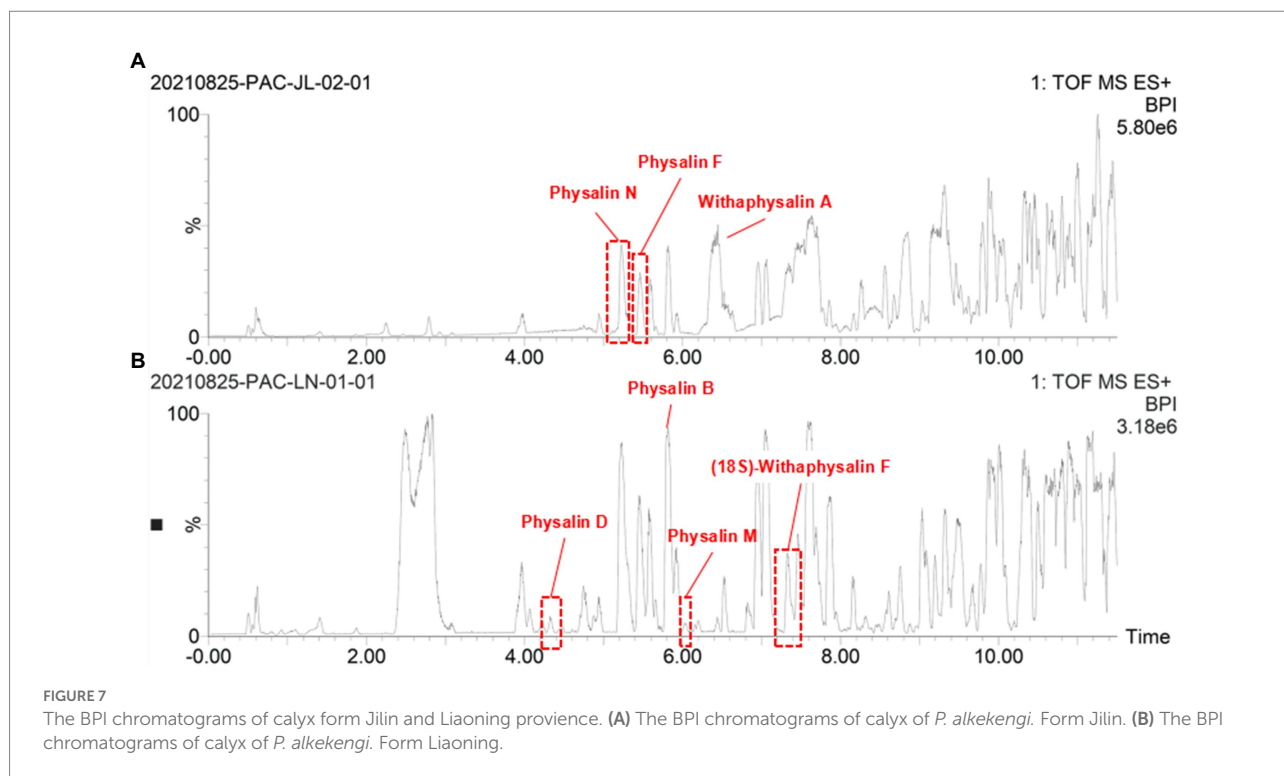
Some traditional Chinese medicinal materials are produced in specific geographic regions with designated

TABLE 3 Candidate gene families associated with physalin biosynthesis.

Description	Enzyme codes	GOs
Demethylase	EC:1.14.11	C:cytosol; F:oxidoreductase activity, acting on paired donors, with incorporation or reduction of molecular oxygen, 2-oxoglutarate as one donor, and incorporation of one atom each of oxygen into both donors; P:oxidation–reduction process
Cytochrome p450	EC:1.14.13	F:oxidoreductase activity, acting on paired donors, with incorporation or reduction of molecular oxygen, NAD(P)H as one donor, and incorporation of one atom of oxygen; F:heme binding; F:iron ion binding; P:oxidation–reduction process
	EC:1.3.3.9	F:heme binding; F:oxidoreductase activity, acting on paired donors, with incorporation or reduction of molecular oxygen; F:monooxygenase activity; F:iron ion binding; P:oxidation–reduction process; F:secologanin synthase activity; P:indole biosynthetic process
	EC:1.14.13.77	F:heme binding; F:iron ion binding; P:oxidation–reduction process; F:taxane 13- α -hydroxylase activity; P:diterpenoid biosynthetic process
	EC:1.14.13.68	F:heme binding; F:iron ion binding; F:hydroxyphenylacetonitrile 2-monooxygenase activity; P:oxidation–reduction process; F:4-hydroxyphenylacetaldehyde oxime monooxygenase activity; P:tyrosine metabolic process
	EC:1.14.13.88	P:floral organ development; P:leaf formation; P:oxidation–reduction process; F:flavonoid 3',5'-hydroxylase activity; P:regulation of meristem growth; P:positive regulation of organ growth; P:regulation of growth rate; F:heme binding; P:positive regulation of cell proliferation; F:iron ion binding; C:endoplasmic reticulum
	EC:1.14.14.1;	F:iron ion binding; F:heme binding; P:fatty acid metabolic process; F:alkane 1-monooxygenase activity; F:aromatase activity;
	EC:1.14.15.3	P:oxidation–reduction process
	EC:1.14.15.3	P:fatty acid metabolic process; F:heme binding; F:iron ion binding; P:oxidation–reduction process; F:alkane 1-monooxygenase activity
	EC:1.14.13.76	F:heme binding; F:taxane 10- β -hydroxylase activity; F:iron ion binding; P:oxidation–reduction process; P:diterpenoid biosynthetic process
	EC:1.14.13.21	F:identical protein binding; P:flavonoid biosynthetic process; F:flavonoid 3'-monooxygenase activity; C:plasma membrane; F:iron ion binding; F:heme binding; F:p-coumarate 3-hydroxylase activity; P:lignin biosynthetic process; P:coumarin biosynthetic process; C:endoplasmic reticulum; C:mitochondrion; P:oxidation–reduction process
	EC:1.14.13.36	F:identical protein binding; P:flavonoid biosynthetic process; F:5-O-(4-coumaroyl)-D-quinic acid 3'-monooxygenase activity; C:plasma membrane; F:iron ion binding; F:heme binding; F:p-coumarate 3-hydroxylase activity; P:lignin biosynthetic process; P:coumarin biosynthetic process; C:endoplasmic reticulum; C:mitochondrion; P:oxidation–reduction process
	EC:1.14.14.1	F:iron ion binding; F:heme binding; C:chloroplast membrane; C:chloroplast stroma; F:aromatase activity; P:oxidation–reduction process
	EC:1.14.14.1;	C:chloroplast envelope; F:zeinoxanthin epsilon hydroxylase activity; F:iron ion binding; F:heme binding; F:aromatase activity;
	EC:1.14.99	P:oxidation–reduction process
	EC:1.6.2.4	C:endoplasmic reticulum membrane; P:response to oxidative stress; F:NADPH-hemoprotein reductase activity; F:iron ion binding; F:FMN binding; C:cytosol; P:response to abscisic acid stimulus; P:oxidation–reduction process; P:electron transport
	EC:1.8.1.7;	P:response to oxidative stress; C:cytosol; P:oxidation–reduction process; F:NADPH-hemoprotein reductase activity;
EC:1.6.2.4	C:peroxisome; P:cell redox homeostasis; P:glutathione metabolic process; F:glutathione-disulfide reductase activity; F:flavin adenine dinucleotide binding; F:NADP binding; C:endoplasmic reticulum membrane; F:iron ion binding; P:response to abscisic acid stimulus; F:FMN binding; P:electron transport; P:gluconeogenesis	
Carboxylesterase	EC:3.1.1.3	F:triglyceride lipase activity; P:lipid catabolic process; P:glycerolipid metabolic process

natural conditions and ecological environments. They are widely recognized as having beneficial clinical therapeutic effects, and are called Daodi medicinal materials, or geoh herbs (Liu et al., 2020). Only the Jilin is regarded as an authentic Daodi production area for *P. alkekengi*. However, it is also found in others of China. In order to investigate the relationship between origins and differential physalin metabolites, we explored differences in the geographic locations of sample collection sites in different areas of China. Only 10 samples were collected from Jilin among all samples. Two batches of samples were divided into groups and their order was randomly assigned within batches. Then, primary phytochemicals and physalin metabolites were detected by UPLC-Q-TOF/MS/MS. MS/MS data was acquired in profile mode, and the MS profile of calyxes from Jilin and other had visible differences (Figure 8).

Additionally, OPLS-DA models were created to separate those two groups further (Figure 9). The VIP was obtained by using OPLS-DA modeling. 20 physalin metabolites among all differential physalins show significant changes (evaluation criteria: VIP > 1), including 6 upregulated metabolites and 12 downregulated metabolites. Based on the accumulation pattern among various metabolites, heatmaps of metabolites were drawn with the OmicStudio tools at <https://www.omicstudio.cn>. using unit variance scaling (UV) and hierarchical cluster analysis (HCA). Calyx samples were also divided into two main groups within HCA. Specifically, samples obtained from Jilin had a significant difference compared to others. The samples from others were further divided into two subgroups. This suggests that those differential physalin metabolites can be employed to distinguish Daodi medicinal properties of *P. alkekengi* and others. In our study, the difference was mainly in expression of withaphysalins and

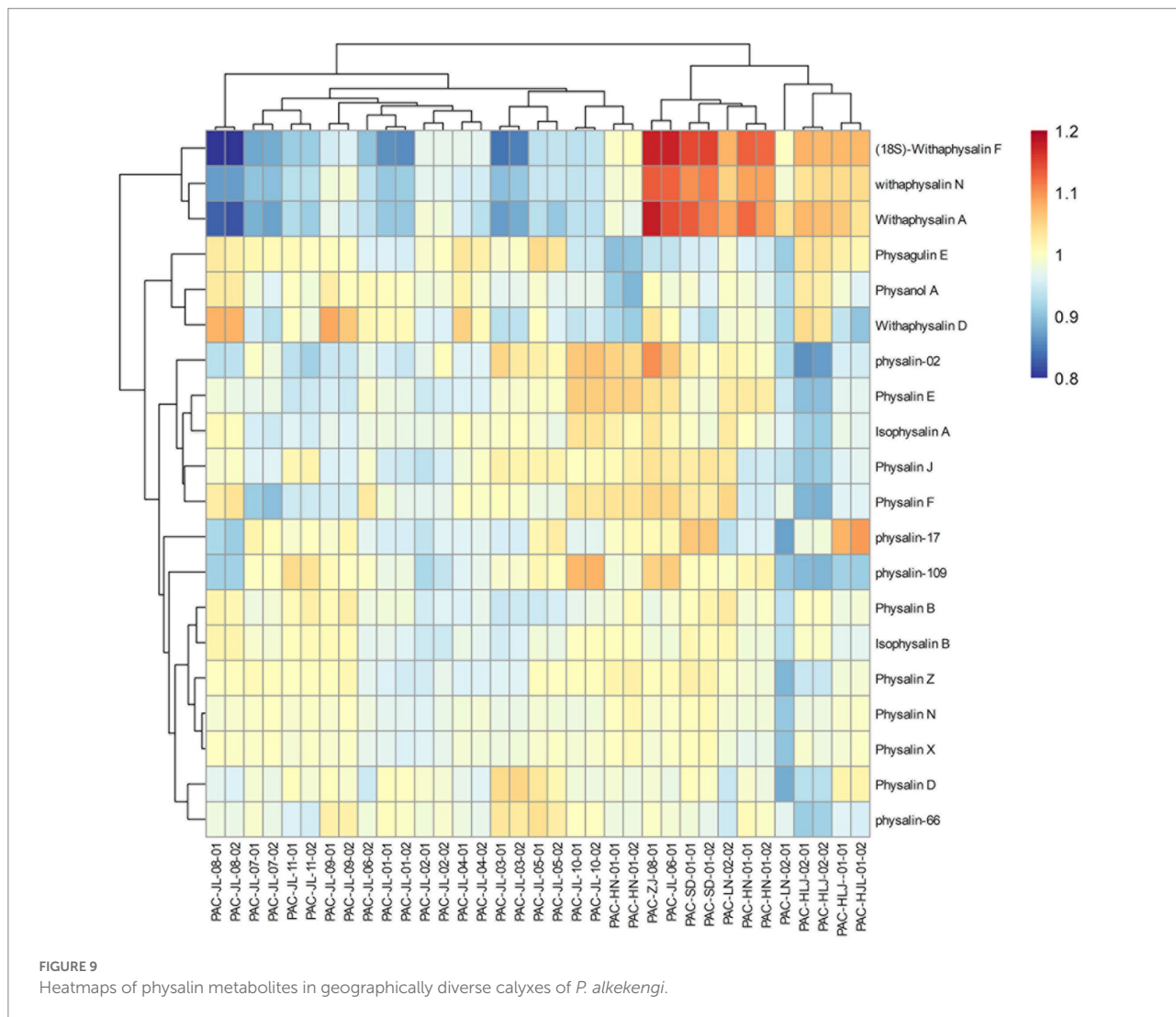


physalins. Quantitative analysis of all components was performed by area normalization using physalin D as the internal standard. Among them, most physalins demonstrated significantly higher contents in the calyces from Jinli vs. Others (Figure 10). However, withaphysalin N, withaphysalin A and (18S)-withaphysalin F demonstrated significantly lower contents (>1.5-fold). Withaphysalins are important intermediates in physalin biosynthetic synthesis, and calyces of *P. alkekengi* from others

consumed more intermediates than those from Jilin. This may lead to fewer physalins being produced.

Conclusion

We used metabolomics to identify the metabolic pathway involved in physalin biosynthesis. In all, 58 different physalin



metabolites have been isolated from *P. alkekengi* calyxes and berries. In an analysis of the physalin biosynthesis pathway, we determined that withanolides and withaphysalins may represent crucial intermediates between lanosterol and physalins, and those steps were decanted according to previous reports. Our results provide valuable information on the physalin metabolites and candidate enzymes involved in the physalin biosynthesis pathways in *P. alkekengi*. In addition, we further analyzed differential metabolites between calyxes from Jilin (Daodi of *P. alkekengi*) and others. Among them, 20 physalin metabolites may represent herb quality biomarkers for Daodi *P. alkekengi*, providing an essential role in directing the quality control index of *P. alkekengi*.

Data availability statement

The datasets for this study can be found in MetaboLights (<https://www.ebi.ac.uk/metabolights/MTBLS5060>).

Author contributions

LYQ: design the experiment, completed the experiments and draft the manuscript. CLG: assisted editing and finalizing the manuscript. XLC: assist in completing the experiment. CCL: assisted in the completion of data processing. LBW: assisted in the completion of data processing. YLW: assisted in the sample collection and validation. JH and JHW: designed the experiments and supervised their completion. All authors contributed to the article and approved the submitted version.

Funding

This work was supported by National Science and Technology Major Project of the Ministry of Science and Technology of China (no. 2018ZX09735005).

Acknowledgments

The authors thank JHW, for support with all study. The authors apologize to all colleagues whose work has not been cited due to space limitations.

Conflict of interest

The authors declare that the research was conducted in the absence of any commercial or financial relationships that could be construed as a potential conflict of interest.

Publisher's note

All claims expressed in this article are solely those of the authors and do not necessarily represent those of their affiliated organizations, or those of the publisher, the editors and the reviewers. Any product that may be evaluated in this article, or claim that may be made by its manufacturer, is not guaranteed or endorsed by the publisher.

References

- Babot, E. D., del Río, J. C., Cañellas, M., Sancho, F., Lucas, F., Guallar, V., et al. (2015). Steroid hydroxylation by basidiomycete peroxigenases: a combined experimental and computational study. *Appl. Environ. Microbiol.* 81, 4130–4142. doi: 10.1128/AEM.00660-15
- Ding, N., Lu, Y., Cui, H., Ma, Q., Qiu, D., Wei, X., et al. (2020). Physalin D inhibits RANKL-induced osteoclastogenesis and bone loss via regulating calcium signaling. *BMB Rep.* 53, 154–159. doi: 10.5483/BMBREP.2020.53.3.147
- Dunn, W. B., and Ellis, D. I. (2005). Metabolomics: current analytical platforms and methodologies. *TrAC-trends. Anal. Chem.* 24, 285–294. doi: 10.1016/j.trac.2004.11.021
- Fukushima, A., Nakamura, M., Suzuki, H., Yamazaki, M., Knoch, E., Mori, T., et al. (2016). Comparative characterization of the leaf tissue of *Physalis alkekengi* and *Physalis peruviana* using RNA-seq and metabolite profiling. *Frontiers. Plant Sci.* 7:1883. doi: 10.3389/fpls.2016.01883
- Gupta, P., Goel, R., Agarwal, A. V., Asif, M. H., Sangwan, N. S., Sangwan, R. S., et al. (2015). Comparative transcriptome analysis of different chemotypes elucidates withanolide biosynthesis pathway from medicinal plant *Withania somnifera*. *Sci. Rep.* 5:18611. doi: 10.1038/srep18611
- Kim, H. B., Schaller, H., Goh, C. H., Kwon, M., Choe, S., An, C. S., et al. (2005). *Arabidopsis cyp51* mutant shows postembryonic seedling lethality associated with lack of membrane integrity. *Plant Physiol.* 138, 2033–2047. doi: 10.1104/pp.105.061598
- Knoch, E., Sugawara, S., Mori, T., Poulsen, C., Fukushima, A., Harholt, J., et al. (2018). Third DWF1 paralog in Solanaceae, sterol $\Delta 24$ -isomerase, branches withanolide biosynthesis from the general phytosterol pathway. *Proc. Natl. Acad. Sci. U. S. A.* 115, 8096–8103. doi: 10.1073/pnas.1807482115
- Last, R. L., Jones, A. D., and Shchar-Hill, Y. (2007). Towards the plant metabolome and beyond. *Nat. Rev. Mol. Cell Biol.* 8, 167–174. doi: 10.1038/nrm2098
- Li, A. L., Chen, B. J., Li, G. H., Zhou, M. X., Li, Y. R., Ren, D. M., et al. (2018). *Physalis alkekengi* L. var. *franchetii* (mast.) Makino: an ethnomedical, phytochemical and pharmacological review. *J. Ethnopharmacol.* 210, 260–274. doi: 10.1016/j.jep.2017.08.022
- Li, X., Zhao, J., Yang, M., Liu, Y., Li, Z., Li, R., et al. (2014). Physalins and withanolides from the fruits of *Physalis alkekengi* L. var. *franchetii* (mast.) Makino and the inhibitory activities against human tumor cells. *Phytochem. Lett.* 10, 95–100. doi: 10.1016/j.phytol.2014.08.004
- Lin, F., and Wang, J. H. (2011). Chemical constituents of physalins from dried calyx of *Physalis alkekengi* var. *franchetii*. *Drugs Clin. 26*, 469–472.
- Liu, X., Zhang, Y., Wu, M., Ma, Z., Huang, Z., Tian, F., et al. (2020). The scientific elucidation of daodi medicinal materials. *Chin. Med.* 15:86. doi: 10.1186/s13020-020-00367-1
- Luo, J. (2015). Metabolite-based genome-wide association studies in plants. *Curr. Opin. Plant Biol.* 24, 31–38. doi: 10.1016/j.pbi.2015.01.006
- Mishra, B., Chand, S., and Singh Sangwan, N. (2019). ROS management is mediated by ascorbate-glutathione- α -tocopherol triad in co-ordination with secondary metabolic pathway under cadmium stress in *Withania somnifera*. *Plant Physiol. Biochem.* 139, 620–629. doi: 10.1016/j.plaphy.2019.03.040
- Misico, R. I., Nicotra, V. E., Oberti, J. C., Barboza, G., Gil, R. R., and Burton, G. (2011). Withanolides and related steroids. *Prog. Chem. Org. Nat. Prod.* 94, 127–229. doi: 10.1007/978-3-7091-0748-5_3
- Oikawa, A., Otsuka, T., Nakabayashi, R., Jikumaru, Y., Isuzugawa, K., Murayama, H., et al. (2015). Metabolic profiling of developing pear fruits reveals dynamic variation in primary and secondary metabolites, including plant hormones. *PLoS One* 10:e0131408. doi: 10.1371/journal.pone.0131408
- Pontrelli, S., Chiu, T. Y., Lan, E. I., Chen, F. Y. H., Chang, P., and Liao, J. C. (2018). *Escherichia coli* as a host for metabolic engineering. *Metab. Eng.* 50, 16–46. doi: 10.1016/j.ymben.2018.04.008
- Roesler, K., Lu, C., Thomas, J., Xu, Q., Vance, P., Hou, Z., et al. (2021). *Arabidopsis* Carboxylesterase 20 binds Strigolactone and increases branches and tillers when ectopically expressed in *Arabidopsis* and maize. *Front. Plant Sci.* 12:639401. doi: 10.3389/fpls.2021.639401
- Sawada, Y., Akiyama, K., Sakata, A., Kuwahara, A., Otsuki, H., Sakurai, T., et al. (2009). Widely targeted metabolomics based on large-scale MS/MS data for elucidating metabolite accumulation patterns in plants. *Plant Cell Physiol.* 50, 37–47. doi: 10.1093/pcp/pcn183
- Sawada, Y., and Yokota Hirai, M. (2013). Integrated LC-MS/MS system for plant metabolomics. *Comput. Struct. Biotechnol. J.* 4:201301011. doi: 10.5936/csbj.201301011
- Shu, Z., Xing, N., Wang, Q., Li, X., Xu, B., Li, Z., et al. (2016). Antibacterial and anti-inflammatory activities of *Physalis Alkekengi* var. *franchetii* and its Main constituents. *Evid. Based Complement. Alternat. Med.* 2016:4359394. doi: 10.1155/2016/4359394
- Sun, C. P., Qiu, C. Y., Zhao, F., Kang, N., Chen, L. X., and Qiu, F. (2017). Physalins V-IX, 16,24-cyclo-13,14-seco withanolides from *Physalis angulata* and their antiproliferative and anti-inflammatory activities. *Sci. Rep.* 7, 4057. doi: 10.1038/s41598-017-03849-9

Supplementary material

The Supplementary material for this article can be found online at: <https://www.frontiersin.org/articles/10.3389/fpls.2022.956083/full#supplementary-material>

SUPPLEMENTARY FIGURE 1

MS spectra of physalin A and fragmentation pattern of the protonated molecular ion. (A) molecular ion peak of physalin A. (B) fragmentation pattern of protonated molecular ion.

SUPPLEMENTARY FIGURE 2

MS spectra of physalin D and fragmentation pattern of the protonated molecular ion. (A) molecular ion peak of physalin D. (B) fragmentation pattern of protonated molecular ion.

SUPPLEMENTARY FIGURE 3

MS spectra of physalin G and fragmentation pattern of the protonated molecular ion. (A) molecular ion peak of physalin G. (B) fragmentation pattern of protonated molecular ion.

SUPPLEMENTARY FIGURE 4

MS spectra of physalin L and fragmentation pattern of the protonated molecular ion. (A) molecular ion peak of physalin L. (B) fragmentation pattern of protonated molecular ion.

SUPPLEMENTARY FIGURE 5

MS spectra of physalin O and fragmentation pattern of the protonated molecular ion. (A) molecular ion peak of physalin O. (B) fragmentation pattern of protonated molecular ion.

SUPPLEMENTARY FIGURE 6

Two fragmentation pathway in parent structure of physalins.

- Urano, K., Kurihara, Y., Seki, M., and Shinozaki, K. (2010). "Omics" analyses of regulatory networks in plant abiotic stress responses. *Curr. Opin. Plant Biol.* 13, 132–138. doi: 10.1016/j.pbi.2009.12.006
- Wu, S. Y., Leu, Y. L., Chang, Y. L., Wu, T. S., Kuo, P. C., Liao, Y. R., et al. (2012). Physalin F induces cell apoptosis in human renal carcinoma cells by targeting NF- κ B and generating reactive oxygen species. *PLoS One* 7:40727. doi: 10.1371/journal.pone.0040727
- Wu, J., Zhang, T., Yu, M., Jia, H., Zhang, H., Xu, Q., et al. (2020). Anti-inflammatory Withanolides from *Physalis minima*. *ACS. Omega* 5, 12148–12153. doi: 10.1021/acsomega.0c00467
- Xu, W. X., Chen, J. C., Liu, J. Q., Zhou, L., Wang, Y. F., and Qiu, M. H. (2013). Three new physalins from *Physalis alkekengi* var. *franchetii*. *Nat. Prod. Bioprospecting* 3, 337–344. doi: 10.1007/s13659-013-0021-z
- Yang, J., Sun, Y., Cao, F., Yang, B., and Kuang, H. (2022a). Natural products from *Physalis alkekengi* L. var. *franchetii* (mast.) Makino: a review on their structural analysis, quality control, pharmacology, and pharmacokinetics. *Molecules* 27:695. doi: 10.3390/molecules27030695
- Yang, J., Tian, J., Yang, Y., Zhu, Y., Li, C., and Zhang, Y. (2022b). RNAi of sterol Δ 24-Isomerase implicated its involvement in Physalin biosynthesis in *Physalis angulata* L. *Front. Plant Sci.* 13:850711. doi: 10.3389/fpls.2022.850711
- Yazaki, K. (2005). Transporters of secondary metabolites. *Curr. Opin. Plant Biol.* 8, 301–307. doi: 10.1016/j.pbi.2005.03.011
- Zhu, F., Dai, C., Fu, Y., Loo, J. F. C., Xia, D., Gao, S. P., et al. (2016). Physalin A exerts anti-tumor activity in non-small cell lung cancer cell lines by suppressing JAK/STAT3 signaling. *Oncotarget* 7, 9462–9476. doi: 10.18632/oncotarget.7051